Modelling Transient Mechanical Behavior of Aluminum Alloy During Electric-Assisted Forming

Jai Tiwari, Hariharan Krishnaswamy, and Murugaiyan Amirthalingam

Abstract Electric-assisted forming is a promising technique in which the mechanical behavior of the materials is altered by the application of electric current during deformation. Advantages of electric-assisted forming include improved ductility, reduction of flow stress, and springback. The alteration in the mechanical behavior is in general linked to Joule's heating due to the lack of comprehensive understanding of the mechanism of electric-assisted deformation. Significant efforts are being made in the field of electroplasticity to propose the existence of additional mechanisms through which the electrical effects on deformation could be better explained by experimental and numerical approaches. However, a consensus is lacking on the governing mechanism and a generalized constitutive model for electroplastic deformation therefore is not yet established. In the present work, two models, namely, Joule's heating-based and dislocation density-based are used to predict the mechanical behavior of aluminium alloy samples subjected to pulsed electric current. The dislocation density-based model superposes the thermal and athermal mechanical behavior independent of the underlying mechanism. Results indicate that an attempt to model the electroplastic behavior purely through Joule's heating produces inconsistent results. It is shown that the Joule's heating model can accurately predict either the temperature history or the mechanical behavior and not concurrently.

Keywords Electric-assisted forming · Constitutive model · Joule's heating · Dislocation density

J. Tiwari (✉) · H. Krishnaswamy
Department of Mechanical Engineering, IIT Madras, Chennai 600036, India
e-mail: me18d006@smail.iitm.ac.in

M. Amirthalingam
Department of Metallurgical and Materials Engineering, Indian Institute of Technology Madras, Chennai 600036, India

K. Inal et al. (eds.), *NUMISHEET 2022*, The Minerals, Metals & Materials Series,
https://doi.org/10.1007/978-3-031-06212-4_10

Introduction

Electric-assisted forming involves the application of electric current during the deformation process. The interaction between the applied current and plastic deformation on the mechanical behaviour is generally referred to as electro-plastic effect. Application of electric current leads to significant improvement in formability [1, 2]. Other advantages of electric-assisted forming include reduction of springback [3] and anisotropy effects [4]. The alteration in the mechanical behavior is in general linked to Joule's heating [5]. However, subsequent efforts in the field have proposed the existence of additional mechanisms. These mechanisms include electron wind effect [6], magnetoplasticity [7], and charge imbalance around the defects [8]. The exact rate-controlling mechanism of the observed behavior is still debatable. Therefore, a comprehensive constitutive model to explain the electroplastic effect is not yet established.

Several efforts in the past have been made to systematically analyze the changes in the mechanical behavior under electric-assisted (EA) deformation. These modelling attempts were focused primarily on the Joule's heating due to the lack of complete understanding of the electroplasticity mechanism. In one such attempt, Kroneberger et al. [9] modelled the electric-assisted upsetting process assuming Joule's heating only. The predicted results were found to be deviating from the experimental results. Subsequent efforts were made to modify the heat transfer parameters [10, 11]. Although they were successful in predicting the temperature profile, none of the above could predict the flow stress softening due to EA deformation. This approach completely ignores the microstructural changes such as dislocation density during EA deformation. Any model [12, 13] that considers only the temperature effect on the mechanical behavior is not sufficient to accurately predict the electroplastic behaviour. Therefore, a model capable of incorporating the changes in mechanical behavior under EA deformation will enable us to understand the mechanisms behind it.

In the present work, two models are considered to evaluate the efficacy of a coupled model to predict the electroplastic behavior. For this purpose, a finite element framework is developed for a coupled electrical–thermal–structural analysis in a commercial software ABAQUS. Firstly, the traditional Joule's heating model is implemented into the framework using the electric–thermal parameters. In the same framework, the dislocation density-based constitutive model coupled with Joule's heating effect is implemented using user material (UMAT) subroutines. In order to estimate the extent of error, the results predicted using the dislocation density model are compared with that predicted assuming traditional Joule's heating.

Modelling the Electroplastic Effect

Joule's Heating Model

In case of electric-assisted deformation, temperature of the specimen increases due to Joule's heating effect. Simultaneously, heat loss to the ambient environment takes place from the specimen. The thermal balance of the specimen can be given as

$$mc_p \Delta T = \zeta I^2 Rt - hA_s(T - T_A), \tag{1}$$

where m, c_p, ΔT, A_s, and T represent mass, specific heat capacity, increase in specimen temperature, surface area, and instantaneous temperature of the specimen, respectively. In the Eq. 1, ζ, h, and T_A represent Joule's heating fraction, overall heat transfer coefficient, and ambient temperature, respectively. From the temperature change (ΔT), the resulting drop in flow stress ($\Delta\sigma$) can be predicted using the high-temperature properties of the specimen, as shown in the literature [14].

Dislocation Density-Based Model

A dislocation density-based constitutive model [15, 16] is used to model the electroplastic behaviour. This model is a simplified form of Kocks–Mecking–Estrin model [17], according to which the flow stress is a function of averaged dislocation density ρ as

$$\boldsymbol{\sigma} = M\alpha Gb\sqrt{\rho}\left(\frac{\dot{\varepsilon}}{\dot{\varepsilon}_0}\right)^{\frac{1}{m}}, \tag{2}$$

where M, G, b, and m are Taylor factor, shear modulus, Burger's vector, and strain rate exponent, respectively. $\dot{\varepsilon}_0$ corresponds to a critical strain rate at which the thermal component of the flow stress reaches to zero. The material constant, α is obtained by curve fitting the experimental stress–strain data. The evolution of dislocation density (ρ) with respect to strain (ε) is given as

$$\frac{d\rho}{d\epsilon} = M(K_1\sqrt{\rho} - K_2\rho), \tag{3}$$

where K_1 and K_2 represent the coefficients of stage-II and stage-III strain hardening, respectively. The parameter K_1 is treated as constant, as the stage-II hardening is athermal in nature. State-III hardening relates to the recovery or annihilation of dislocations. Therefore, the coefficient K_2 relies on temperature and strain rate. It can be represented [17] as

$$K_2 = (K_2)_0 \left(\frac{\dot{\varepsilon}}{\dot{\varepsilon}_0} \right)^{-\frac{1}{n}}, \tag{4}$$

where $(K_2)_0$ is a material constant and the exponent n depends on temperature.

In Eq. 2, m and α and $\dot{\varepsilon}$ depend on the temperature and strain rate. Similarly, n in Eq. 4 depends on temperature. In order to avoid complexity, the rate dependency of m and $\dot{\varepsilon}_0$ is coupled with that of α [16]. Therefore, α and n can be modelled as

$$\alpha = \alpha_0 \beta_1 \left\{ \dot{\varepsilon}^{\beta_2} T^{\beta_3} \right\}, \tag{5}$$

$$n = \beta_6 \left\{ T^{\beta_7} \right\}, \tag{6}$$

where α_0, β_1, β_2, β_3, β_6, and β_7 are material constants.

The rate-dependent parameters (α and n) can be further modified to include the effect of electric current. The following relation, which was originally proposed in [15], is utilized in the present work.

$$\alpha = \alpha_0 \beta_1 \left\{ \dot{\varepsilon}^{\beta_2} T^{\beta_3} + \frac{\beta_4}{\beta_1} J^{\beta_5} \right\}, \tag{7}$$

$$n = \beta_6 \left\{ T^{\beta_7} + \frac{\beta_8}{\beta_6} J^{\beta_9} \right\}, \tag{8}$$

where the constants β_4, β_5, β_8, and β_9 are used to describe the electroplastic effect for a current density J. The procedure to obtain the above-mentioned parameters is explained in our recent work [18].

A two-parameter dislocation–density model was proposed to account for the recovery in pulsed mode. In that case, the total dislocation density is decomposed to forward (ρ_f) and reverse (ρ_r) components [16]. In the present work, if $\overset{\circ}{\rho}_f$ is the total dislocation density at a given strain corresponding to the application of electric pulse, the ρ_f and ρ_r are given by

$$\rho_f = (1 - p) \overset{\circ}{\rho}_f, \tag{9}$$

$$\rho_r = p \overset{\circ}{\rho}_f, \tag{10}$$

where 'p' is a scalar indicating the fraction of reverse dislocation split from the total dislocation density during the reduction of electric current density. ρ_r decreases with strain and its evolution is given by

$$\frac{\mathrm{d}\rho_r}{\mathrm{d}\varepsilon} = -q M K_1 \sqrt{\rho_f} \frac{\rho_r}{\overset{\circ}{\rho}_f} \tag{11}$$

where the scalar 'q' corresponds to the rate of evolution of reverse dislocation.

The flow stress in Eq. 2 is modified as

$$\sigma = M\alpha Gb\left(\frac{\dot{\varepsilon}}{\dot{\varepsilon}_{\text{ref}}}\right)^{1/m}\sqrt{\rho_f - \rho_r} \tag{12}$$

When scalars p and q become zero, $\rho_r = 0$ and the governing equations return to the continuous current application case.

The model superposes the thermal and athermal mechanical behavior independent of the underlying mechanism by modifying the variables n and α.

Finite Element Framework

Steps followed in the finite element modelling of electric-assisted deformation are described below:

1. A real scale model of the cylindrical specimen was created with a length of 15 mm and diameter of 10.2 mm. Specimen, upper platen, and lower platen were modelled to simulate the experimental setup, as shown in Fig. 1.
2. Eight-node general-purpose linear brick element (C3D8) is used to carry out the FE analysis. A suitable mesh size (0.5 mm) for the modeled specimen is chosen after a detailed mesh convergence study.
3. A fully coupled thermal–electrical–structural analysis is performed due to the necessity of coupling between the displacement, temperature, and electric fields to obtain solutions for all three fields simultaneously.
4. Fixed boundary condition (displacements and rotations are restricted) is imposed on the lower platen and the boundary condition of the upper platen is given in such a way that the specimen could move only in the axial direction. The cross-head speed was maintained at 2 mm/min during the simulation.
5. The specimen and the platens are bonded using the TIE constraint option. The TIE constraint bonds surfaces together so that there is no relative motion between them. Also, the contact between the platens and specimen is considered to be perfect in the present analysis.
6. The electric current amplitude is converted to the instantaneous current density and applied as electrical load at the top of the specimen. The bottom side of the specimen is grounded to ensure the flow of the electric current in die–specimen assembly.
7. Temperature evolution during EA deformation was measured using a non-contact type FLIR-T621 infrared camera.
8. High-temperature stress–strain behavior of the material is taken from the reference [19]. The thermophysical properties of the material and overall heat transfer coefficient used in the present framework are given in Table 1.

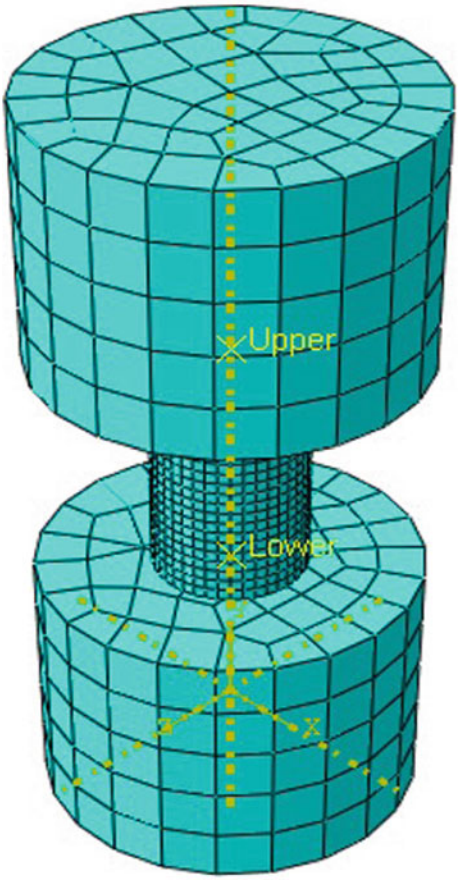

Fig. 1 Setup assembly of platen and specimen used in the finite element analysis is shown

Table 1 Properties used in the present framework

Specific heat (C_p) (J kg^{-1} K^{-1})	Thermal conductivity (k) (W m^{-2} K^{-1})
929–0.627*T	25.2 + 0.398*T
Joule heating fraction (ζ)	Overall heat transfer coefficient (h) (*10^3, W m^{-1} K^{-1})
0.9	0.765

Results and Discussion

In the present work, Joule's heating model and the dislocation density model are evaluated using the pulsed current-assisted results of AA 60661-T6 alloy published in the literature [20]. The present analysis is performed till a strain of 0.2 to avoid any potential fracture. As mentioned in literature [20], nominal electric current densities of 75 and 90 A/mm^2 are applied for a duration of 0.5 s with a background time of 29.5 s for the pulsed current-assisted tests.

In order to obtain the Joule's heating fraction and overall heat transfer coefficient, iterative FE simulations were performed to match the experimentally observed temperature history. Predicted temperature history in case of current density, J = 90 A/mm^2; fits satisfactorily with the experimental profile as shown in Fig. 2. Subsequently, the FE simulation is carried out at a nominal current density of 75 A/mm^2 with the same modelling parameters. The resulting stress–strain behavior along with the experimental results are shown in Fig. 3. It is clear from Fig. 3 that Joule heating model produces inconsistent results while describing stress–strain behavior under electric-assisted deformation.

In the same FE framework, the dislocation density-based constitutive model is implemented using user material (UMAT) subroutines. The fitting constants used in the model are tabulated in Table 2. The predicted stress–strain behavior is presented along with the experimental results in Fig. 4.

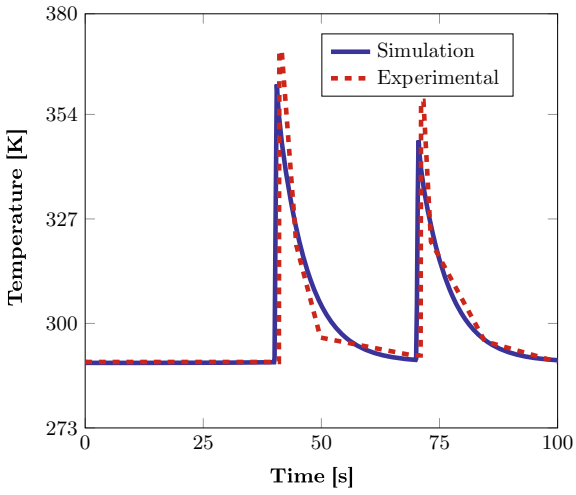

Fig. 2 FE simulation result of temperature profile is plotted with the experimentally recorded temperature history

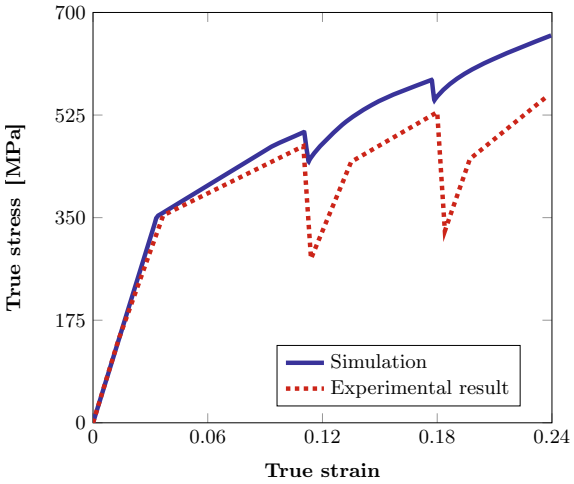

Fig. 3 FE simulation result of temperature profile is plotted with the experimentally recorded temperature history

Table 2 Parameters used in the dislocation density model [21]

M	α_0	G (MPa)	b (mm)	K_1	K_{20}	m	$\epsilon_{\dot{0}}$ (S^{-1})	ρ_0 (mm^{-2})	β_1
3.5	0.45	27,000	$2.86*10^{-7}$	5000	55	2.2	$1.5*10^{-7}$	$7.67*10^5$	1
β_2	β_3	β_4	β_5	β_6	β_7	β_8	β_9	p	q
–0.33	–0.5	–0.065	0.31	0.22	0.42	0.35	0.1	0.3	1

Fig. 4 FE simulation result of temperature profile is plotted with the experimentally recorded temperature history

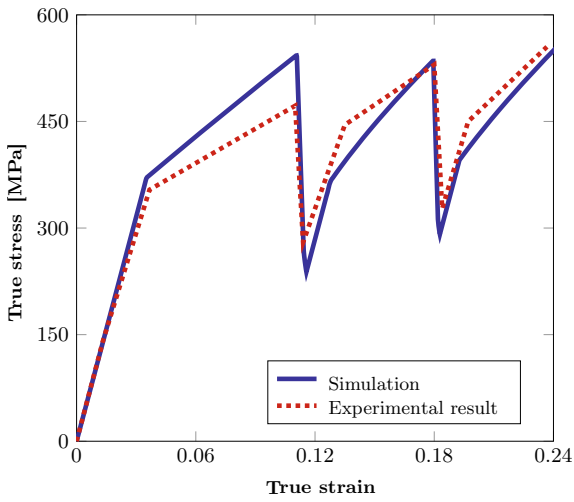

Conclusion

In the present work, two models to predict the electroplastic behaviour have been examined in the same finite element framework. It is observed that the Joule heating model could not accurately predict the temperature profile and stress–strain behavior concurrently. The limitation of Joule's heating model is overcome by the use of modified dislocation density model. This constitutive model in conjunction with Joule's heating effect predicts the mechanical behavior of aluminum alloys under electric-assisted deformation satisfactorily.

Acknowledgements Authors would like to acknowledge the financial support from the Science and Engineering Research Board (Project reference: CRG/2019/0D3539), Department of Science and Technology (DST), India.

References

1. Roth JT, Loker I, Mauck D, Warner M, Golovashchenko SF, Krause A (2008) In: Transactions of the North American manufacturing research institution of SME, pp 405–412
2. McNeff PS, Paul BK (2020) J Alloy Compd 829:154438
3. Lee J, Bong HJ, Lee YS, Kim D, Lee MG (2019) Metall Mater Trans A 50(6):2720
4. Pleta AD, Krugh MC, Nikhare C, Roth JT (2013) In: ASME 2013 international manufacturing science and engineering conference collocated with the 41st North American manufacturing research conference, p V001T01A018
5. Goldman P, Motowidlo L, Galligan J (1981) Scripta Metallurgica 15(4):353
6. Conrad H (2000) Mater Sci Eng: A 287(2):276
7. Molotskii M, Fleurov V (1995) Phys Rev B 52(22):15829
8. Kim MJ, Yoon S, Park S, Jeong HJ, Park JW, Kim K, Jo J, Heo T, Hong ST, Cho SH et al (2020) Appl Mater Today 21:100874
9. Kronenberger TJ, Johnson DH, Roth JT (2009) J Manuf Sci Eng 131(3):031003
10. Hariharan K, Lee MG, Kim MJ, Han HN, Kim D, Choi S (2015) Metall Mater Trans A 46(7):3043
11. Ruszkiewicz BJ, Mears L, Roth JT (2018) J Manuf Sci Eng 140(9)
12. Salandro WA, Bunget C, Mears L (2010) In: ASME 2010 international manufacturing science and engineering conference. American Society of Mechanical Engineers, pp 581–590
13. Magargee J, Fan R, Cao J (2013) J Manuf Sci Eng 135(6)
14. Salandro WA, Bunget CJ, Mears L (2012) Proceedings of the institution of mechanical engineers. Part B: J Eng Manuf 226(5):775, 031003
15. Kim MJ, Lee MG, Hariharan K, Hong ST, Choi IS, Kim D, Oh KH, Han HN (2017) Int J Plast 94:148
16. Krishnaswamy H, Kim MJ, Hong ST, Kim D, Song JH, Lee MG, Han HN (2017) Mater Des 124:131
17. Estrin Y (1996) Unified constitutive laws of plastic deformation 1:69
18. Tiwari J, Pratheesh P, Bembalge O, Krishnaswamy H, Amirthalingam M, Panigrahi S (2021) J Mater Res Technol 12:2185
19. Dorbane A, Ayoub G, Mansoor B, Hamade R, Kridli G, Imad A (2015) Mater Sci Eng: A 624:239
20. Hong ST, Jeong YH, Chowdhury MN, Chun DM, Kim MJ, Han HN (2015) CIRP Ann 64(1):277
21. Tiwari J, Balaji V, Krishnaswamy H, Amirthalingam M (2022) International Journal of Mechanical Sciences, p 107433